LITHOS 448-449 (2023) 107171

Contents lists available at ScienceDirect

LITHOS

journal homepage: www.elsevier.com/locate/lithos

Estimation of P-T entrapment conditions of a subduction fluid using elastic thermobarometry: A case study from Cabo Ortegal Complex, Spain

Tamás Spránitz [a,b], Csaba Szabó [a,b], Mattia Gilio [c], Matteo Alvaro [c], Michaela Blažeková [d], Patrik Konečný [d], Tamás Váczi [e], Márta Berkesi [a,b,*]

[a] Lithosphere Fluid Research Lab, Department of Petrology and Geochemistry, Institute of Geography and Earth Sciences, Eötvös Loránd University, Pázmány Péter sétány 1/C, Budapest 1117, Hungary
[b] MTA FI Lendület FluidsByDepth Research Group, Institute of Earth Physics and Space Science (EPSS), Csatkai Endre utca 6-8, Sopron 9400, Hungary
[c] Department of Earth and Environmental Sciences, University of Pavia, Pavia, Italy
[d] State Geological Institute of Dionýz Štúr, Bratislava 817 04, Slovakia
[e] Institute for Solid State Physics and Optics, Wigner Research Centre for Physics, P.O. Box 49, Budapest H-1121, Hungary

ARTICLE INFO

Keywords:
Elastic thermobarometry
Subduction fluid
Entrapment condition
Quartz-in-garnet
Zircon-in-garnet
Ti-in-quartz

ABSTRACT

Fluid and mineral inclusions in metamorphic rocks allow the understanding of fluid-involved processes in subduction-zones providing essential contributions to the nature of geochemical processes and element cycling in present day subduction zones. In this work, we studied ultramafic granulite from the high-pressure (HP) and high-temperature (HT) metamorphic series of the Cabo Ortegal Complex, Spain, combining quartz-in-garnet and zircon-in-garnet Raman spectroscopy-based elastic geothermobarometry with Ti-in-quartz trace element thermometry. The studied quartz and zircon inclusions occur within garnet, together with rutile and multiphase fluid inclusions (MFI). Textural evidence, like occurrence in the same 3D cluster and common intergrowth of mineral inclusions, shows that both crystal inclusions and MFI were likely entrapped simultaneously. Hence, the application of elastic thermobarometry to quartz and zircon inclusions in these rocks provides excellent opportunity to define P-T environment of entrapment. Results from Raman spectroscopy on multiple quartz and zircon inclusions showed that the remnant elastic inclusion pressure (P_{inc}) at room conditions for both (on average 0.51 ± 0.04 GPa and 0.72 ± 0.05 GPa for the quartz and zircon inclusions, respectively) fall within the range of 2σ uncertainty confirming the crystallization within the same growth-stage of garnet. Intersection of the entrapment isomekes is at a P-T of 1.8 ± 0.2 GPa and 880 ± 70 °C. Electron microprobe measurements on quartz inclusions from the same garnet zone show uniform Ti concentrations (45–59 ppm). Isopleths calculated from Ti-in-quartz thermometer intersect the average quartz-in-garnet isomeke within the P-T range indicated by the intersection of quartz and zircon entrapment isomekes, which is $P = 1.8 \pm 0.2$ GPa and $T = 860 \pm 70$ °C.

Besides, we made a comparison of different reference materials applied for zircon-in-garnet elastic thermobarometry verified by independent Ti-in-quartz trace element thermometry. Our findings indicate that elastic thermobarometry on mineral inclusions provide a reliable constraint on the entrapment P-T conditions of coexisting fluid inclusions.

1. Introduction

Metamorphic processes affect the mineralogy, rheology and density of the Earth's lithosphere and control global geochemical cycles of numerous elements. They are greatly influenced by interactions between fluids (in particular aqueous or carbon-bearing fluids) along tectonically produced shear or fracture zones as metamorphic reactions are greatly accelerated by the presence of fluids compared to tectonically induced changes in pressure and temperature (Jamtveit et al., 2016). The accurate characterization of the chemical composition as well as the pressure and temperature (P-T) of fluid migration events in a fossil subduction zone yields substantial contribution to understand the nature and timing of fluid processes in present-day subduction zones. One of the best candidates for direct records or remnants of subduction fluid events are inclusions trapped in minerals of (ultra)high pressure – (ultra)high temperature (UHP-UHT) metamorphic rocks. This

* Corresponding author at: Institute of Earth Physics and Space Science (EPSS), Csatkai Endre utca 6-8, Sopron 9400, Hungary.
E-mail addresses: berkesi.marta@epss.hu, marta.berkesi@ttk.elte.hu (M. Berkesi).

https://doi.org/10.1016/j.lithos.2023.107171
Received 12 September 2022; Received in revised form 6 April 2023; Accepted 7 April 2023
Available online 11 April 2023

type of fluid inclusions can be highly variable in chemical composition and room temperature phase assemblage, for instance, solute-bearing aqueous-carbonic fluid inclusions (e.g., Hermann et al., 2006; Scambelluri and Philippot, 2001), multiphase solid or fluid inclusions (e.g., Carvalho et al., 2020; Frezzotti and Ferrando, 2015; Hermann et al., 2013; Maffeis et al., 2021; Spránitz et al., 2022), or glassy to crystallized melt inclusions (e.g., Bartoli and Cesare, 2020; Cesare et al., 2015; Ferrero and Angel, 2018).

Multiphase solid and fluid inclusions found in (U)HP-(U)HT rocks have commonly experienced post-entrapment modifications, such as re-equilibration including fluid/host mineral interaction accompanied by partial fluid loss via long-term exhumation processes (Bodnar, 2003; Carvalho et al., 2020; Frezzotti and Ferrando, 2015; Maffeis et al., 2021; Spránitz et al., 2022). Mapping such inclusions, using 2D or 3D imaging with Raman spectroscopy and Focused Ion Beam Scanning Electron Microscopy (FIB-SEM), provides the possibility to describe the post-entrapment modifications, additionally to estimate initial composition of the fluid (Carvalho et al., 2020; Maffeis et al., 2021; Spránitz et al., 2022). There is, however, no direct record for the successful re-homogenization of such inclusions, which could offer a direct way to obtain entrapment P-T conditions.

In this paper, we discuss the entrapment P-T conditions of garnet-hosted multiphase fluid inclusions (MFI) in a granulite from the Cabo Ortegal Complex (NW-Spain) using elastic and chemical properties of mineral inclusions co-entrapped with MFI. Mineral inclusions are ubiquitous in metamorphic rocks over wide range of P-T conditions and may develop residual pressure within the host mineral upon exhumation (Alvaro et al., 2020; Mazzucchelli et al., 2018; Kohn et al., 2023). According to differences in thermodynamic properties between host and inclusion, some host-inclusion systems are good barometers (e.g., quartz-in-garnet) whereas others (e.g., zircon-in-garnet) are good thermometers (Gilio et al., 2022). Thus, the coexistence of these phases within a single host allows the corresponding isomekes (the line of possible entrapment) to intersect and define a unique point of entrapment in *P–T* space (Gilio et al., 2022). In this contribution, we provide an application of quartz-in-garnet and zircon-in-garnet elastic Raman thermobarometry supported by Ti-in-quartz trace element thermometry. This indirect approach can serve as a promising way to estimate fluid entrapment conditions for those (U)HP-(U)HT inclusions that cannot be conventionally re-homogenized.

2. Geology and sampling

The Cabo Ortegal Complex of the Iberian Massif is an assemblage of high-pressure and high-temperature (HP-HT) metamorphic units interpreted as fragments of continental and oceanic lithosphere, formerly being involved in a Devonian subduction-exhumation cycle (Ábalos et al., 2003; Puelles et al., 2005). The studied area is a remnant of a fossil subduction zone (Ábalos et al., 2003) and it mainly consists of eclogites, granulites, peridotites and pyroxenites, ortho- and paragneisses and metagabbros (Gil Ibarguchi et al., 1990; Puelles et al., 2005). These units show geological characteristics of different origins in oceanic, arc or continental settings. They share a common high-grade tectonometamorphic evolution in a subduction-zone, recording a metamorphic peak between 380 and 395 Ma (Ábalos et al., 2003). Peak metamorphic conditions for the main units have been determined as follows: eclogite (1.8–2.2 GPa, 700–800 °C), granulite (1.4–1.8 GPa, 740–835 °C), peridotites and pyroxenites (1.6–1.8 GPa, 780–800 °C), gneiss (ca. 1.5 GPa, 700 °C) (Ábalos et al., 2003; Gil Ibarguchi et al., 1990; Puelles et al., 2005; Tilhac et al., 2017).

The HP granulite-facies ensemble, known as the Bacariza Formation, is a heterogeneous lithostratigraphic unit in the Cabo Ortegal Complex dominated by garnet- and plagioclase-rich lithotypes, including granulitic orthogneisses, ultramafic, Mg-rich mafic, intermediate and common mafic granulites, but the protolith of each subtype of granulite is still not fully constrained (Galán and Marcos, 1997, 2000; Gil Ibarguchi et al., 1990; Puelles et al., 2005). Plagioclase-poor mafic-ultramafic granulites, termed as pyrigarnites by Vogel (1967), the subject of this work, are defined as rocks having commonly a compositional banding that may evolve into nearly monomineralic domains consisting of almost exclusively garnet, alternating with others rich in clinopyroxene or into bimineralic garnet- and clinopyroxene-rich domains (Puelles et al., 2005). Therefore, strictly based on modal compositions, some of them could be considered as garnet pyroxenites, however all HP granulites have undergone metamorphism under fairly the same P-T conditions (Puelles et al., 2005). Garnet pyroxenite also occur as dykes in the Cabo Ortegal Complex within the pyroxenite unit (structurally clearly distinct from granulites), however they correspond to magmatic origin by the injection of mafic melts during peak metamorphic conditions (Santos et al., 2002; Tilhac et al., 2017). Previous studies indicate an independent origin and distinct protolith of granulites and eclogites, thus the HP granulite metamorphism is considered as part of a single cycle in a subduction conduit setting and precluding interpretation supporting the origin of granulites after eclogites (Puelles et al., 2005). All of this made reasonable to apply the conventionally used terminology (i.e., ultramafic granulite) for the studied rock.

The studied ultramafic granulites are composed mainly of garnet and clinopyroxene with minor amounts of plagioclase and rutile (Galán and Marcos, 1997; Puelles et al., 2005). Garnet, showing weak normal zoning within the compositional range of $Alm_{38–55}Grs_{17–32}Prp_{15–34}And_{2–13}Sps_{1–4}$, often exhibits a concentric arrangement of inclusions due to growth stages (Beranoaguirre et al., 2020; Puelles et al., 2005), i.e., core and inner zones contain primary MFI along with abundant crystal inclusions such as quartz, rutile and zircon (Spránitz et al., 2022). These MFI, built up by step-daughter minerals (Fe-Ca-Mg-carbonates, pyrophyllite, quartz, corundum ± graphite) together with a residual fluid phase of $CO_2 + N_2 \pm CH_4$ are products of post-entrapment reactions of an originally homogeneous COHN fluid with the garnet host (Spránitz et al., 2022). This fluid was dominated by H_2O and CO_2 with no sign of trapped melt phase, afterwards involved in fluid-host reactions with the garnet (Spránitz et al., 2022). Calculations suggested that the original fluid was trapped likely around peak conditions (ca. 1.8 GPa and 800 °C). Despite a detailed characterization of post-entrapment history of these inclusions, only little information is available about their HP-HT formation conditions. Microthermometry on these MFI, using a heating stage with no pressure medium, failed due to either poor visibility and/or decrepitation before homogenization.

The studied granulite sample derives from one of the major outcrops of the Bacariza Formation (Fig. 1), from the same location (N43° 42.722' W7° 58.330′) described in Spránitz et al. (2022) as COC17-079a, as well as previously by Galán and Marcos (1997) as AMP-450.

3. Analytical methods

Petrographic observations (Fig. 2) were done using a Nikon Opti-Phot2 optical microscope equipped with a Nikon CooplPix DS-Fi1 camera in the Lithosphere Fluid Research Lab, Eötvös University, Budapest. Micro-Raman spectroscopic analysis was carried out using a HORIBA JobinYvon Labram HR (high resolution) 800 spectrometer with Nd-YAG laser ($\lambda = 532$ nm) excitation at the Research and Industrial Relations Center of the Faculty of Science, Eötvös University, Budapest. The analytical settings included 50–100 μm confocal hole, 60–150 s acquisition time, 3× accumulations, 100× objective and application of different filters to avoid sample overheating during the Raman measurements (Zhong et al., 2019). Spectral resolution of the measurements was ~0.7 cm^{-1} with the applied grating of 1800 grooves/mm based on the full width at half maximum (FWHM) value of the emission band of a Ne lamp at 540.06 nm. Instrumental precision was about 0.37 cm^{-1}, which refers to the half of the spectral pixel-to-pixel distance resulting from several instrumental factors, thus this value is applied as the uncertainty of Raman measurement as used by Campomenosi et al. (2020)

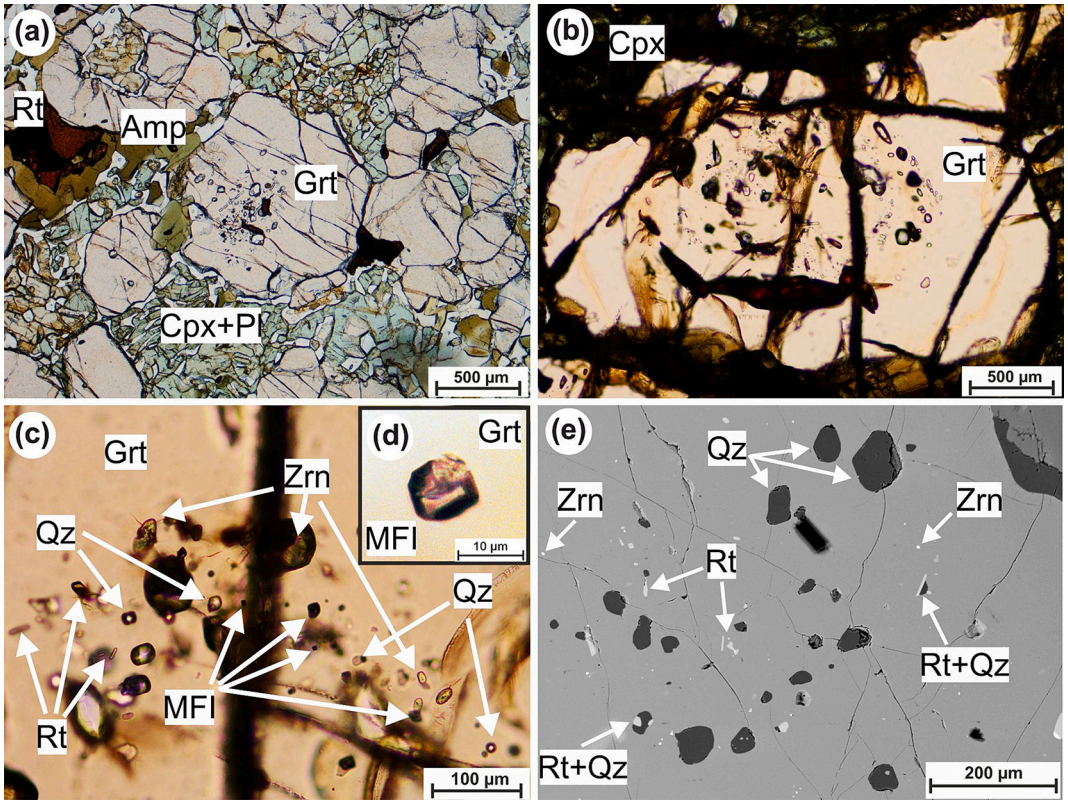

Fig. 1. Photomicrographs showing characteristic petrographic features of the studied granulite. (a) Textural feature of the rock-forming minerals, indicating modal garnet-dominance, (b) Garnet showing an inclusion-rich core (multiphase fluid inclusions (MFI) and crystal inclusions such quartz, rutile and zircon), (c) Higher magnification image of the inclusion-rich zone of garnet including abundant MFI, quartz, zircon and rutile crystal inclusions, (d) Close-up image of primary MFI with negative crystal shape, formed by multiple solid and fluid phases, (e) Back-scattered electron image of quartz and rutile inclusion intergrowth within the same growth-zone of garnet. Abbreviations: garnet (Grt), quartz (Qz), rutile (Rt), zircon (Zrn), clinopyroxene (Cpx), plagioclase (Pl), amphibole (Amph), multiphase fluid inclusions (MFI).

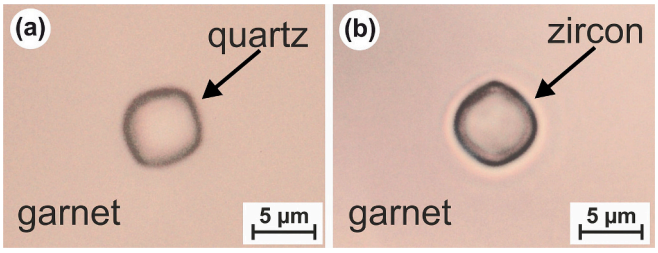

Fig. 2. Representative photomicrographs (using transmitted light) of the selected, garnet-hosted quartz (a) and zircon (b) crystal inclusions from the studied granulite of the Cabo Ortegal Complex.

and Gilio et al. (2021, 2022). Data were collected in the spectral range of 100–1100 cm^{-1}. Reference crystals with the same acquisition settings and emission bands of the Ne lamp were measured several times (after every second inclusion) during each measurement session for precise wavenumber calibration and to have control on band position shifting due to daily instrumental stability. Free crystals were used as references to define Raman shift of the inclusions, such as a free-standing (unstrained) quartz crystal removed from the studied rock and two different zircon crystals. Two measurement sessions were carried out on the same zircon inclusions using different reference crystals, both fitting the criteria established by Campomenosi et al., 2020. In the first session (referred to be as synthetic zircon reference in Table S2) the zircon reference was a pure (undoped), flux-grown synthetic zircon crystal synthetized with the method described by Hanchar et al. (2001). In the second session (referred to be as a natural zircon reference in Table S2), a reference zircon from Ratanakiri, Cambodia was used. This zircon is known to be highly ordered with no noticeable amounts of radiation damage and low Hf content (<0.7 wt%) (Nasdala et al., 2018; Zeug et al., 2018). Raman shifts near 128, 206, 263 and 464 cm^{-1} of quartz and near 201, 213, 224, 356, 438, 975 and 1009 cm^{-1} of zircon were measured to determine inclusion strain using the stRAinMAN software (Angel et al., 2019). Following the guidelines of Angel et al. (2019), the concept of phonon-mode Grüneisen tensor was applied to obtain full strain state of the inclusions and providing less uncertainty than calculating directly from single-mode shifts with the assumption of hydrostatic stress in the inclusions (Gilio et al., 2022). We selected for elastic geothermobarometry only the zircons with FWHM at the shift near 1009 < 5 cm^{-1} (Campomenosi et al. (2020). In agreement with Bonazzi et al. (2019), Campomenosi et al. (2018) and Mazzucchelli et al. (2018), Raman spectra were acquired from the center of the inclusions to avoid inclusion shape effects. Raman spectra were processed using the software OriginPro 2018. Raman spectra were baseline-corrected for their luminescence background, temperature-reduced to account for the Bose-Einstein occupation factor (Kuzmany, 2009) and normalized to the acquisition time. Peak positions, full-widths at half maximum (FWHMs) and integrated intensities were determined from fits with pseudo-Voigt functions.

Residual strain was calculated using Raman shift of band positions near 128, 206, 263 and 464 cm^{-1} for quartz and near 438, 975 and 1009 cm^{-1} for zircon inclusions compared to the same ones of reference crystals (Fig. 3). We selected these three modes as they are the internal modes corresponding to Si—O bending, symmetric and antisymmetric stretching of zircon, respectively and discarded the external modes to minimize compositional effects such as high Hf content (Campomenosi

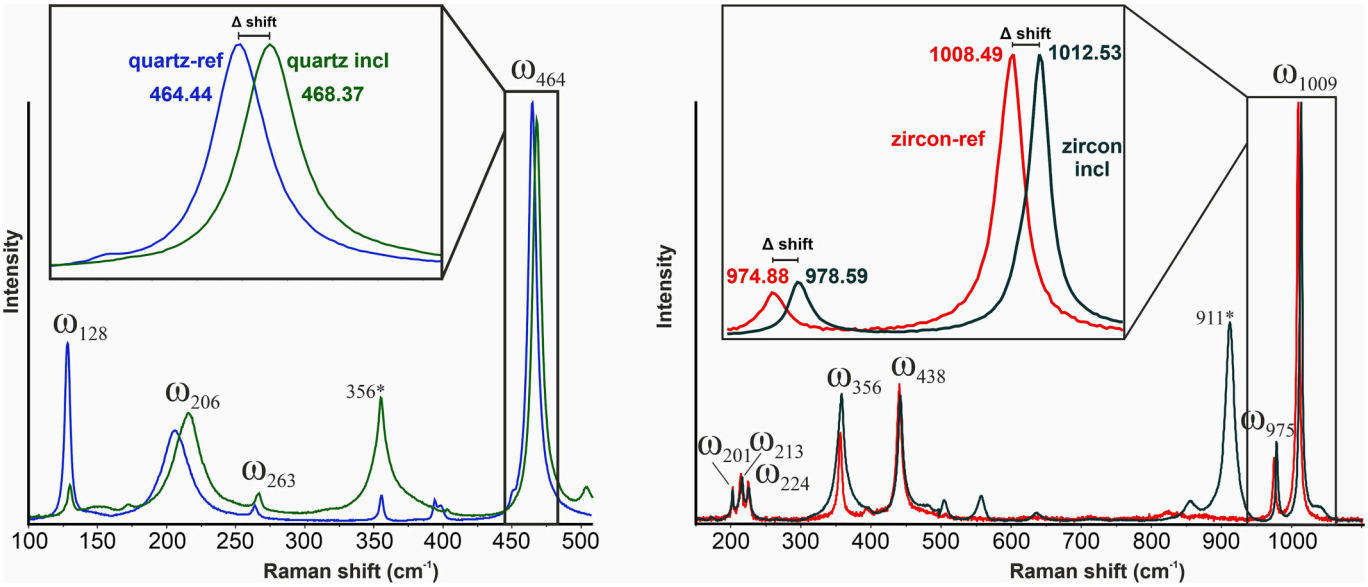

Fig. 3. Representative Raman spectra showing the differences in the band positions of characteristic Raman modes of the reference crystals and the studied quartz (left) and zircon (right) inclusion preserving residual strain. This figure shows the Raman band positions of zircon inclusions in comparison to natural (Ratanakiri) zircon crystal as applied for further calculations. The Raman bands of the host garnet at 356 cm^{-1} and 911 cm^{-1} are marked with asteriks.

et al., 2020). Residual pressure of quartz and zircon inclusions was calculated using their Grüneisen tensors (Murri et al., 2018; Stangarone et al., 2019) with the software EntraPT (https://www.mineralogylab.com/software/entrapt/; Mazzucchelli et al., 2021) from the residual strain. Residual strain was converted to residual stress using the available elastic tensors (Wang et al. (2015) and Özkan et al. (1974) for quartz and zircon, respectively). The inclusion pressure was calculated for each inclusion as mean normal stress ($(\sigma_1 + \sigma_2 + \sigma_3)/3$). To calculate P-T conditions of entrapment, we applied the approach of isotropic – full strain – approximation (Angel et al., 2014) as the uncertainties of strain measured with Raman spectroscopy are too large to apply the anisotropic approach (Alvaro et al., 2020; Gilio et al., 2021, 2022).

The chemical compositions of quartz, garnet and zircon were analyzed using a CAMECA-SX100 wavelength-dispersive electron microprobe in State Geological Institute of Dionýz Štúr, Bratislava, Slovakia. Accelerating voltage of 15 kV was applied to all mineral phases. Measurement of titanium in quartz inclusions used for Ti-in-quartz thermometry requires applying highly stable measurement conditions and specialized analytical procedure involving 180 nA beam current for Ti and long measurement time for counting on the Ti lasting in total ca. 12 min. Counting time on peak and two backgrounds was 240 and 200 s, respectively. Contents of Al in quartz inclusions were measured using also 180 nA beam current and Si were measured with 20 nA beam current. All quartz inclusions were measured with 10 μm beam diameter. The following analytical conditions were applied for garnet: 4 μm beam diameter, 20 nA beam current and 15 kV accelerating voltage, each measurement lasting for 3 mins. Zircon inclusions were measured using 15 kV accelerating voltage, 20 nA beam current with 5 μm beam diameter, each measurement lasting for 15 mins. Further details on analytical conditons, such as standards, crystals, lines and detection limits are included in Supplementary material 1.

3.1. Rock and inclusion petrography

The studied ultramafic granulite has moderately sheared granoblastic texture dominated by euhedral garnet (up to 1 mm in diameter) and anhedral clinopyroxene together with minor amounts of plagioclase, rutile and quartz (Fig. 1). As a common retrograde microstructure (Puelles et al., 2005), secondary clinopyroxene and plagioclase, forming fine-grained symplectitic aggregates, are also frequent. Garnet has a core rich in quartz, zircon and rutile inclusions occurring together with primary MFI in the same growth zone of garnet (Fig. 1). These mineral inclusions commonly occur intergrown with each other, supporting simultaneous entrapment. Quartz inclusions range in size from 5 up to 150 μm and characterized mostly by euhedral shape, whereas zircon occurs as 5–80 μm spherical-elongated crystals (Fig. 2). Measured quartz inclusions ($n = 14$) have radii of 2 to 10 μm with an average of 5 μm, whereas the radii of zircons ($n = 7$), ranged between 3 and 12 μm averaged with 5 μm (for more details of selection criteria, see Supplementary material 1 and Fig. S1).

3.2. Major and trace element analyses

Electron probe micro-analyses (EPMA) was applied to measure major, minor elements in the host garnet, and minor to trace elements in exposed quartz and zircon inclusions (Table 1 and S1). All garnet corresponds to almandine-rich composition ($Alm_{47\text{-}50}Grs_{18\text{-}25}Prp_{23\text{–}27}And_{0\text{–}2}Sps_{1\text{–}2}$) and may show weak normal zoning with a slight increase of Fe and Mg and decrease of Ca from core to rim, which is consistent with previous results of Puelles et al. (2005) (Table S1, Fig. S2). Measurement of Ti concentration in 25 quartz inclusions, exposed on the sample surface in the studied growth zone of garnet, was carried out to perform Ti-in-quartz geothermometry. These analyses were done on inclusions of a diameter at least 10 μm, not intimately intergrown or close to neighboring rutile or zircon inclusions to avoid possible "contamination" of other inclusions and the host garnet. Zircon inclusions contain low amounts of Hf and U, making them eligible for calculations using elastic thermobarometry (Campomenosi et al., 2020; Nasdala et al., 2002). Concentration of Hf and U varies in the range between 1.04 and 1.35 wt%, and maximum 0.19 wt%, respectively. In average, most of U content falls at or below detection limit that is 690 ppm (2σ) (Table S1).

4. Results

4.1. Elastic Raman thermobarometry of quartz and zircon inclusions

The results of Raman measurements on quartz and zircon inclusions, as well as the reference crystals are shown on Figs. 3-4 and summarized in Table S2. The average of P_{inc} for quartz inclusions is 0.51 ± 0.04 GPa.

Table 1
Ti concentration (ppm) in quartz inclusions and temperature estimates using calibration method of Thomas et al. (2010). Uncertainty propagation of temperature estimates was calculated using the method of Taylor (1997).

Analyses	TiO_2 (wt%)	Ti (ppm)	det limit (ppm)	2σ (ppm)			Thomas et al. (2010)					
					Mole fraction	Uncertainty	5 kbar	10 kbar	15 kbar	20 kbar	25 kbar	2σ
COC17-079a_Ti in qtz term_an1–1	0.0084	50	10	9	6.27964E-05	1.13039E-05	580	680	790	900	1000	30
COC17-079a_Ti in qtz term_an2–1	0.0098	59	10	9	7.4099E-05	1.13039E-05	590	700	810	920	1020	30
COC17-079a_Ti in qtz term_an3–1	0.0084	50	10	9	6.27964E-05	1.13039E-05	580	680	790	900	1000	30
COC17-079a_Ti in qtz term_an4–1	0.0093	56	10	9	7.03315E-05	1.13039E-05	590	690	800	910	1020	30
COC17-079a_Ti in qtz term_an5–1	0.0093	56	10	9	7.03315E-05	1.13039E-05	590	690	800	910	1020	30
COC17-079a_Ti in qtz term_an5–2	0.0096	58	10	9	7.28431E-05	1.13039E-05	590	700	810	910	1020	30
COC17-079a_Ti in qtz term_an5–3	0.0097	58	10	9	7.28431E-05	1.13039E-05	590	700	810	910	1020	30
COC17-079a_Ti in qtz term_an6–1	0.0088	53	10	9	6.6564E-05	1.13039E-05	580	690	800	900	1010	30
COC17-079a_Ti in qtz term_an7–1	0.0096	58	10	9	7.28431E-05	1.13039E-05	590	700	810	910	1020	30
COC17-079a_Ti in qtz term_an8–1	0.0091	55	10	9	6.90756E-05	1.13039E-05	580	690	800	910	1010	30
COC17-079a_Ti in qtz term_an9–1	0.0086	52	10	9	6.53081E-05	1.13039E-05	580	690	790	900	1010	30
COC17-079a_Ti in qtz term_an10–1	0.0088	53	10	9	6.6564E-05	1.13039E-05	580	690	800	900	1010	30
COC17-079a_Ti in qtz term_an10–2	0.0081	48	10	9	6.02847E-05	1.13039E-05	570	680	780	890	1000	30
COC17-079a_Ti in qtz term_an11–1	0.0079	47	10	9	5.90289E-05	1.13039E-05	570	680	780	890	990	30
COC17-079a_Ti in qtz term_an12–1	0.0091	55	10	9	6.90756E-05	1.13039E-05	580	690	800	910	1010	30
COC17-079a_Ti in qtz term_an13–1	0.0084	50	10	9	6.27964E-05	1.13039E-05	580	680	790	900	1000	30
COC17-079a_Ti in qtz term_an14–2	0.0085	51	10	9	6.40523E-05	1.13039E-05	580	680	790	900	1000	30
COC17-079a_Ti in qtz term_an14–3	0.0074	45	10	9	5.65171E-05	1.13039E-05	570	670	780	880	990	30
COC17-079a_Ti in qtz term_an15–1	0.0089	53	10	9	6.6564E-05	1.13039E-05	580	690	800	900	1010	30
COC17-079a_Ti in qtz term_an15–2	0.0078	47	10	9	5.90289E-05	1.13039E-05	570	680	780	890	990	30
COC17-079a_Ti in qtz term_an19–1	0.0094	57	10	9	7.15873E-05	1.13039E-05	590	700	800	910	1020	30
COC17-079a_Ti in qtz term_an20–1	0.0091	54	10	9	6.78198E-05	1.13039E-05	580	690	800	900	1010	30
COC17-079a_Ti in qtz term_an21–1	0.0096	58	10	9	7.28431E-05	1.13039E-05	590	700	810	910	1020	30
COC17-079a_Ti in qtz term_an22–1	0.0087	52	10	9	6.53081E-05	1.13039E-05	580	690	790	900	1010	30
COC17-079a_Ti in qtz term_an23–1	0.0076	46	10	9	5.7773E-05	1.13039E-05	570	670	780	890	990	30
average	0.0085	53					580	690	800	900	1010	30

Residual strain for zircon was calculated in two measurement sessions on the same set of inclusions using different reference material (synthetic and natural zircon crystal, for details see Methods). Raman spectra of these two crystals (Table S2) indicate negligible effect of radiation damage, i.e., position and FWHM of the Raman band near 1009 cm^{-1} (Campomenosi et al., 2020; Zhong et al., 2019). Even though, they show systematic and notable shift in the position of all Raman bands relative to each other, such as a shift of ~1 cm^{-1} for the band near 1009 cm^{-1} (i.e., 1007.5 cm^{-1} for the synthetic and 1008.5 cm^{-1} for the natural zircon crystal, Table S2). Such discrepancy of the reference crystals results in different shifts for each Raman mode for the same inclusions, and thus different values for P_{inc}, i.e. 0.84 ± 0.05 GPa, using the synthetic, and 0.72 ± 0.05 GPa, using the natural reference crystal (Table S2).

The P_{inc} of quartz and zircon are consistent within their 2σ uncertainty (Fig. 4, Table S2), thus their average can be used to calculate an isomeke representative for their entrapment (Gilio et al., 2022). Isomekes for the garnet end-members (almandine, grossular, and pyrope) were calculated with software EntraPT using the newly formulated EoS by Angel et al. (2022). Starting from the end-member isomeke, we calculated an isomeke for quartz and for zircon to account for the garnet composition ($Alm_{0.51}Prp_{0.26}Grs_{0.23}$) following the procedure described in Angel et al. (2022).

4.2. Independent constraint on entrapment temperature: Ti-in-quartz thermometry

According to EPMA analysis, concentration of Ti in quartz ranges between 45 and 59 ppm with an average of 53 ppm (Table 1). Occurrence within the same growth zone of garnet and common intergrowth with rutile inclusions indicate Ti-saturation during quartz crystallization, therefore TiO_2 activity can be considered equal to 1 (i.e. $\alpha^{rutile}_{TiO2} = 1$).

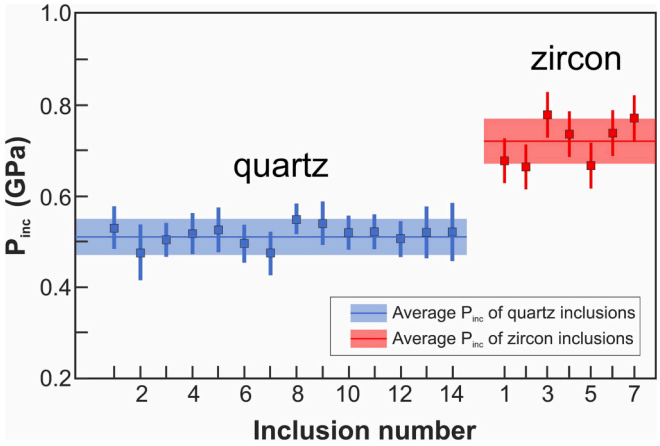

Fig. 4. Residual pressure (P_{inc}) measured in individual quartz (blue squares) and zircon (red squares) inclusions in garnet from granulite of the Cabo Ortegal Complex. Lines with transparent bars represent the average and uncertainty of the P_{inc} for quartz (blue) and zircon (red) inclusions, respectively (Table S2). Note that P_{inc}, calculated from residual strain, corresponds to the inclusion pressure at room conditions. It was used to back-calculate the entrapment isomekes, applied as thermobarometers (sub-horizontal line for quartz and high angle for zircon), using thermodynamic properties of the host and the inclusions (Angel et al., 2014, 2017). (For interpretation of the references to colour in this figure legend, the reader is referred to the web version of this article.)

Crystallization temperature was estimated using Ti-in-quartz solubility model of Thomas et al. (2010), as calculation of Ti-in-quartz isopleths using this calibration, has good control on the dependence of pressure. Calculation of Ti-in-quartz concentrations showed an average crystallization temperature of 580 ± 30 °C at 0.5 GPa, 690 ± 30 °C at 1.0 GPa, 800 ± 30 °C at 1.5 GPa and 900 ± 30 °C at 2.0 GPa (Table 1, Fig. 5.).

5. Discussion

Inclusion petrography of the studied granulite clearly suggests that mineral inclusions such as quartz, rutile and zircon trapped coevally with MFI, during the same growth-stage of host garnet (Fig. 1). Applying thermobarometry on these mineral inclusions provide excellent opportunity to calculate not only entrapment P-T condition of both crystal inclusions, but also the coexisting COHN subduction fluid (Spránitz et al., 2022). In general, the estimation of P-T conditions of fluid events of the metamorphic rock is challenging as MFI cannot be homogenized and quenched like the (U)HT melt-rich inclusions using a pressure medium, i.e., the piston cylinder apparatus (e.g., nanogranitoids, Bartoli and Cesare, 2020). This is because COHN fluid will not form a glass phase by rapid cooling followed by homogenization. Moreover, H_2O is likely partially lost from MFI after entrapment (Spránitz et al., 2022), thus a homogenization experiment would not be representative of the initial fluid. P-T estimations from independent material, like the coevally entrapped mineral inclusions, offers a fine tool to overcome the abovementioned obstacles. Our approach was, therefore, to combine quartz-in-garnet and zircon-in-garnet elastic geothermobarometry with Ti-in-quartz thermometry to 1) test and verify the applicability of elastic thermobarometry on our sample, and 2) combine the results with the previous thermodynamic calculations and available P-T data of the studied rock.

5.1. Reequilibration at peak metamorphic conditions?

The effect of chemical and mechanical reset due to diffusion and non-elastic relaxation should be considered when interpreting any kind of geothermobarometry on granulites (e.g., Frost and Chacko, 1989; Spear and Florence, 1992; Zhong et al., 2018, 2020). Even if such effects cannot be fully neglected on the studied materials, both petrographic observations and the results in light of the exhumation history of the area (Ábalos et al., 2003; O'Brien and Rötzler, 2003), rather support the idea that the studied inclusions have preserved both chemical and elastic data characteristic of their entrapment.

Even though Ti diffusion in quartz is expected to be very fast at HT conditions, limited information is available about whether equilibrium between garnet and the enclosed quartz inclusion could be achieved as Ti diffusion in garnet is infinitely slow (Spear et al., 2012). Quartz may also keep Ti concentration acquired during prograde path in garnet without evident sign of resetting (Gonzalez et al., 2019; Jeanneret et al., 2022; Johnson et al., 2021; Spear et al., 2023). This is supported by the fact that neither variations of Ti concentration within quartz, nor anomalous Ti concentrations were observed adjacent to the inclusions in the host garnet. Thus, no reset at peak metamorphic conditions is rather suggested.

Our results on chemical zoning pattern of garnet, containing abundant fluid and mineral inclusions in the core, agree with previous studies of Puelles et al. (2005), showing weak prograde zoning with a slight increase of Fe and Mg and decrease of Ca from core to rim. It also indicates non-reequilibrated garnet chemistry. Preservation of mineral compositions from peak conditions and even prograde path is characteristic for Variscan high-pressure granulites as they experienced fast cooling during rapid exhumation (O'Brien and Rötzler, 2003). In these cases, pre-peak garnet compositions might also be preserved and not homogenized at peak conditions as it is generally presumed for granulite facies garnets (Cooke, 2000; O'Brien, 2001; O'Brien and Rötzler, 2003). Such evolution corresponds well with data on rapid cooling and exhumation of the Cabo Ortegal Complex (Ábalos et al., 1996, 2003; Galán and Marcos, 2000; Ordóñez Casado et al., 2001 and Puelles et al., 2005).

Non-elastic reset of zircon inclusions may also depend on the P-T path followed by the rock after entrapment rather than the absolute temperature only (Campomenosi et al., 2022). They showed that, if the exhumation path is 'shallower' than the entrapment isomeke, zircon inclusions remain in the compressional domain enhancing the preservation of original residual pressure. In other words, if steepness of entrapment isomeke of the zircon-in-garnet is flatter than that of the exhumation path, as highly likely for the studied rock (Fig. 5), the calculated P_{inc} record true entrapment conditions, similarly as evidenced by Gilio et al. (2022). Such post-entrapment evolution of the inclusions correspond with the available data for cooling rate of the studied rocks as peak metamorphic conditions were followed by rapid cooling and exhumation with minimum rates of ca. 90 °C/Ma and ca. 5.8 km/Ma (Ordóñez Casado et al., 2001).

Fluid inclusions trapped along the prograde metamorphic path, (i.e., prior to peak conditions) become internally overpressurized and would suffer high strain before reaching maximum P-T conditions (Sterner and Bodnar, 1989). Such inclusions are characterized by fractures starting from the corners and haloes of secondary inclusions surrounding the original inclusion (Bodnar, 2003). This texture is absent from the studied sample and the primary MFI are intact indicating that they have not likely experienced significant overpressure after entrapment, making it possible to survive and preserve such intact shape as shown on Fig. 1d. In other words, fluid inclusion petrography supports entrapment near peak P-T conditions (Fig. 5) with no traces of reequilibration.

5.2. Application of elastic thermobarometry coupled with trace element thermometry

In this study, the isotropic approximation method (Angel et al., 2014) was applied to calculate the lines of possible entrapment in P-T space, i.e., isomekes from residual strain measured in multiple inclusions in garnet. Intersection of zircon-in-garnet and quartz-in-garnet entrapment isomekes, calculated from the corresponding average P_{inc}, provides a single point of entrapment (Fig. 4, Table S2). This approach (the isotropic approximation) has been proposed as the most reliable

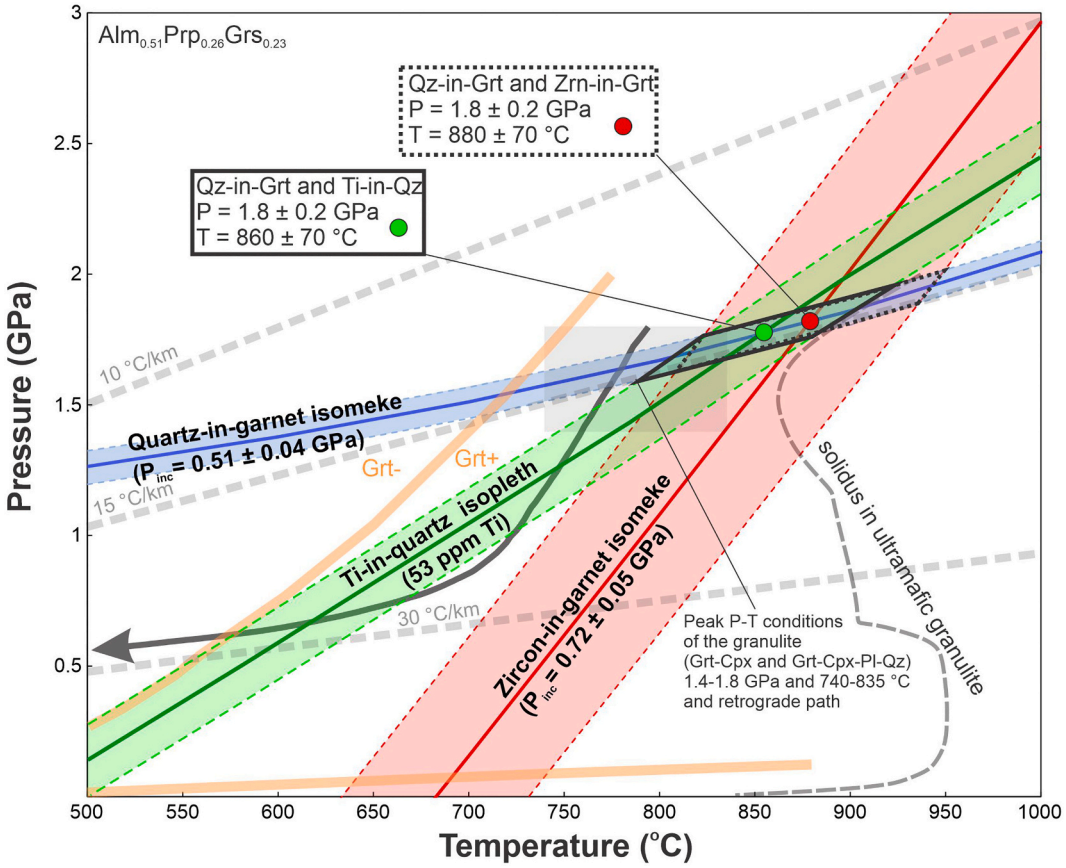

Fig. 5. Pressure vs. temperature diagram demonstrating the entrapment conditions (rectangle with black colour frame) of coexisting quartz (blue line) and zircon (red line) inclusions marked by the intersection of their isomeke. The green line represents isopleth of Ti concentration in quartz inclusions. Shaded green, red and blue areas bracketed with dashed lines indicate the range of uncertainty of the Ti-in-quartz isopleth and the P_{inc}, respectively (see Table 1 and S2 for the data). Orange thick lines with Grt- and Grt + show P-T range denoted by the equilibrium of garnet and the trapped COHN fluid based on thermodynamic modelling using bulk MFI compositions (Spránitz et al., 2022). The solidus curve corresponds to the anatexis of a HP-HT ultramafic granulite (Ferrero et al., 2018) with highly similar modal and bulk chemical composition to the studied sample. Peak metamorphic conditions and retrograde path of the granulite are based on Puelles et al. (2005). Grey dashed lines represent geothermal gradients at 10 °C/km, 15 °C/km, and 30 °C/km, respectively, corresponding to thermobaric ratios at 335 °C/GPa, 500 °C/GPa, and 1000 °C/GPa. (For interpretation of the references to colour in this figure legend, the reader is referred to the web version of this article.)

method to estimate entrapment conditions in quartz-garnet and zircon-garnet inclusion-host systems if calculating with negligible effects of plastic or viscous deformation of inclusions (Angel et al., 2017; Gilio et al., 2021, 2022; Mazzucchelli et al., 2021).

Besides chemical and elastic reset from entrapment to peak T, various processes, like shape maturation, viscous creep or plastic flow during decompression may lead to a pressure drop and reset of strain in quartz inclusions trapped during the prograde-to-peak metamorphic path, thus an underestimation of residual pressures (Cesare et al., 2021; Zhong et al., 2020).

Our results, however, indicate that the selected quartz inclusions preserve highly similar residual pressure based on the narrow range of P_{inc} values (Fig. 4, Table S2), which would imply simultaneous entrapment without the evidence of partial reset during retrograde metamorphic path. Moreover, the calculated average quartz isomeke intersects the P-T path near peak metamorphic conditions (cc. 1.6 GPa, Fig. 5, Puelles et al., 2005). This suggests that the studied quartz inclusions have experienced no or only minor post-entrapment reequilibration during the retrograde path. This is also supported by the observation that bigger, irregular-shaped quartz inclusions with cuspate-like necks showed significantly smaller (i.e., a difference of 3–4 cm^{-1} in the Raman band near 206 cm^{-1}) difference in Raman shifts from the reference crystal than the studied inclusions. Detailed characterization of these latter inclusion types, likely experienced reequilibration during exhumation is out of the scope of this paper.

Plastic relaxation and a reset of the original entrapment pressure of zircon may be related to the P-T path of the rock after inclusion entrapment (post-entrapment heating and/or decompression; Campomenosi et al., 2022) that is unlikely considering the exhumation path of the Cabo Ortegal Complex (see above in section 6.1). Residual pressure of zircon inclusions was calculated using two different pure reference crystals characterized by slightly different Raman band positions (Table S2). This resulted in significantly different P_{inc} values for the same set of inclusions that is an average of 0.12 GPa, which corresponds to almost a 200 °C difference using the equation of state of almandine (Table S2). The P_{inc} obtained by calculating with the synthetic zircon crystal, however, shows unrealistically high values (0.84 ± 0.05 GPa), which would imply entrapment conditions of min. ca. 900 °C at 1.6 GPa calculating with a pure pyrope endmember host (Gilio et al., 2021). Note that garnet composition has an important effect on the predicted entrapment temperature in case of zircon inclusions, caused by distinct thermal expansion coefficient of the endmembers, such as a difference of ca. 200 °C at 1 GPa for pure almandine or pure pyrope endmembers (Angel et al., 2022). Considering the measured average garnet composition ($Alm_{0.51}Prp_{0.26}Grs_{0.23}$), this would account for entrapment temperatures higher than ca. 1000 °C. Consequently, in the followings, we discuss only the results of calculations using the natural zircon reference crystal. The intersection of zircon-in-garnet isomeke using the natural reference material with the quartz-in-garnet isomeke is at P-T of 1.8 ± 0.2 GPa and 880 ± 70 °C.

Previous studies showed that not only the degree of metamictisation, but also the incorporation of non-formula elements in the zircon crystal structure might modify the zircon Raman spectrum (Hoskin and Rodgers, 1996). Zircon, containing 1.63 wt% Hf and 0.6 wt% U, show only a minor deviation in Raman band positions from a pure crystal that is <1 cm^{-1} (Nasdala et al., 2002). Therefore, our results on EPMA measurements of exposed zircon inclusions imply negligible effects of minor elements on zircon Raman shifts as they contain 1.04–1.35 wt% Hf, and up to 0.19 wt% U (Table S1).

Inclusion entrapment P-T conditions are additionally constrained by the crossing point of quartz-in-garnet isomekes and Ti-in-quartz isoplets, which serve as an independent thermometer to validate zircon-in-garnet elastic thermometry. The application of Ti-in-quartz geothermometer is a common method used to obtain P-T estimates of crystallization as quartz occurs in most crustal rocks over a wide range of P-T conditions (e.g., Thomas et al., 2010; Tual et al., 2018). Recently, it has been successfully applied not only on matrix quartz, but on inclusions trapped in garnet (Gonzalez et al., 2019). The intersection point of the average Ti concentration isopleth and average quartz-in-garnet isomeke is interpreted to represent P-T conditions of garnet growth and quartz inclusion entrapment, i.e., at $P = 1.8 \pm 0.2$ GPa and $T = 860 \pm 70$ °C (Fig. 5). This P-T range shows a striking overlap of the one provided by the intersection of quartz-in-garnet and zircon-in-garnet isomekes (Fig. 5). Such independent constraint confirms that calculations of zircon-in-garnet thermometry, using the Ratanakiri zircon as a natural reference crystal, provide reliable results on entrapment temperature.

5.3. Subduction fluid event during granulite facies metamorphism

Based on complementary elastic and trace element thermobarometry, the studied mineral inclusions have been trapped at the P-T range of 1.8 ± 0.2 GPa and ca. 870 ± 70 °C (Fig. 5). The obtained entrapment conditions show good agreement with peak metamorphic conditions estimated for the studied granulite, especially in terms of pressure (Puelles et al., 2005, Fig. 5). Our results show slightly higher (i.e., on average 870 ± 70 °C) temperature than reported for the granulite by Puelles et al. (2005) (790 ± 50 °C, Fig. 5), although considering the error of the estimations, the temperature ranges show significant overlap. However, the temperature range obtained here extends to slightly higher temperatures, therefore our results might indicate that high-pressure granulite facies conditions could have reached higher temperatures with even ca. 80 °C than estimated previously.

Granulite facies peak metamorphism is commonly accompanied by the presence of melt phase, as these conditions are commonly positioned above the solidus of the bulk rock on the P-T space. Melting is also evidenced by the presence of melt inclusions in high-grade rocks, such as migmatites, granulites and anatectic enclaves (Cesare et al., 2015). Nevertheless, neither nanogranitoid inclusions (i.e, anatectic melt enclosed in peritectic minerals) nor any petrographic evidence of partial melting was observed in the studied rock, which is anyway fundamentally rare for (ultra)mafic HP granulites (Ferrero et al., 2018). This was confirmed by preceding thermodynamic modelling that a homogeneous COHN fluid should have been in equilibrium with the host garnet at HP-HT conditions (Spránitz et al., 2022). Therefore, P-T curve of the solidus of the studied ultramafic granulite can be considered as the upper limit of fluid phase entrapment for our case, which can be placed at ca. 910 °C at 1.8 GPa based on results on thermodynamic modelling of ultramafic granulite with highly similar modal and bulk composition to the studied one (see sample AMP-450 in Galán and Marcos, 1997 and Ferrero et al., 2018).

The originally trapped fluid indicates CO_2 dominance with minor H_2O (Spránitz et al., 2022), which is in agreement with fluid compositions recorded during granulite facies metamorphism (Crawford and Hollister, 1986). Fluids are thought to play key role in granulite facies peak metamorphism, involving the mechanism of infiltration of externally derived chemically active CO_2-rich fluids with low H_2O activity (Newton et al., 1998; Rajesh and Santosh, 2012; Touret, 2009). The influx of such fluids, migrating along some fissure or crack and subsequently outwards along the mineral grain boundaries of the surrounding rock, is likely to promote a fluid induced solid-state dehydration resulting in the breakdown of such hydrous minerals as biotite or amphibole to form clinopyroxene and/or orthopyroxene (Harlov, 2012). Occurrence of abundant rutile and zircon inclusions in garnet as inclusion-rich domains (Fig. 1) might confirm this interpretation. They are possibly related to the prograde growth of garnet at the expense of former Ti-bearing phase (probably biotite or amphibole) as described in Variscan mafic high-pressure granulites showing a P-T path during subduction-exhumation processes comparable to the Cabo Ortegal Complex (O'Brien, 2008).

5.4. Method to estimate subduction fluid entrapment

Our study indicates that the application of comprehensive elastic geothermobarometry can be a useful tool to obtain reasonable entrapment conditions of the coexisting fluid inclusions. Calculation of inclusion strain using the concept of phonon-mode Grüneisen tensor (Murri et al., 2018) and the isotropic method to determine entrapment isomeke (Angel et al., 2017) allowed to acquire reliable estimates on equilibration pressure and temperature as proposed by guidelines of Gilio et al. (2021, 2022), which is also supported by the agreement of chemical (Ti-in-quartz) with elastic thermometry (Fig. 5). Relying on petrographic evidences on MFI together with the exhumation history of the area, we calculated with only minor or negligible effects of resetting of inclusion pressures after entrapment (Campomenosi et al., 2021, 2022; Cesare et al., 2021; Ferrero and Angel, 2018; Zhong et al., 2020).

Application of quartz-in-garnet, zircon-in-garnet combined with Ti-in-quartz thermobarometry to many igneous and metamorphic rocks is accessible as garnet, quartz, rutile and even zircon are common in many bulk compositions crystallizing over a wide range of P-T conditions (Gonzalez et al., 2019). Furthermore, garnet acts as a common host mineral for fluid and/or melt inclusions together with mineral inclusions such as quartz ± zircon in a wide variety of (U)HP-(U)HT metamorphic rocks from several localities (e.g., Carvalho et al., 2020; Ferrando et al., 2009; Groppo et al., 2009).

Even though having some direct records of the remnants of supercritical fluids from (U)HP rocks, represented by multiphase solid inclusions (Frezzotti and Ferrando, 2015), they rarely preserve the original composition as their present-day composition is usually dry already. An alternative and promising direct way to re-homogenize and study the nature of (U)HP-(U)HT inclusions at entrapment conditions could be the application of hydrothermal diamond anvil cell (HDAC) experiments. Such in situ analyses could be applied successfully on those inclusions, which are likely to have preserved their original composition, in particular in terms of H_2O content, e.g., multiphase solid inclusions from UHP garnet orthopyroxenites of the Maowu Ultramafic Complex, China (Malaspina et al., 2017) or multiphase solid inclusions from UHP eclogite of the Sulu terrain, China (Zhang et al., 2008). However, compared to conventional techniques, experiments with HDAC provide the outstanding opportunity to observe and study in situ the behavior of various fluid systems at high P and T (e.g., Li and Chou, 2017), several issues still have to be addressed during homogenization of multiphase inclusions, such as e.g.: 1) avoid decrepitation with proper external pressure and heating rate, 2) uncertainty about the possibility to reverse step-daughter producing fluid-host reactions, 3) overcome metastability of solid phases. Preliminary P-T estimates measured in coexisting mineral inclusions using elastic thermobarometry would make a reliable base to establish experiments with HDAC as requiring no homogenization of the fluid.

Our findings indicate that elastic thermobarometry on certain mineral inclusions may provide reasonable constraint on P-T conditions of fluid entrapment during subduction zone conditions. The advantage of the use of Raman spectroscopy is being simple, fast, optically controlled,

non-destructive (repeatable) (Bodnar and Frezzotti, 2020). Application of high-resolution 2D and 3D Raman imaging, showing excellent agreement in volume proportions obtained by means of FIB-SEM analyses, provide a detailed characterization of inclusions with complex phase assemblage that is crucial to reconstruct their bulk composition (Aradi et al., 2022; Carvalho et al., 2020; Spránitz et al., 2022).

All of this implies that it is worth taking the time for a careful check if (U)HP-(U)HT, likely multiphase fluid inclusions occur together with tiny (<10 μm) mineral inclusions, such as quartz and/or zircon, as they likely preserve valuable information about fluid entrapment. The obtained P-T estimates provide a contribution to the nature and timing of subduction fluid processes, which is of great importance to better understand subduction zone metamorphism and global element cycling.

6. Conclusions

In this study, we applied elastic thermobarometry and Ti-in-quartz trace element thermometry on quartz and zircon inclusions in garnet, trapped together with MFI, in granulite from the Cabo Ortegal Complex. The major findings of our research are summarized as follows:

- Elastic thermobarometry on quartz and zircon inclusions allowed us to estimate their entrapment P-T conditions during host garnet growth without any evidence of resetting. Intersection of the entrapment isomekes is at a pressure and temperature of 1.8 ± 0.2 GPa and 880 ± 70 °C, respectively. These values highly likely correspond to peak conditions of granulite facies metamorphism.
- Isopleths calculated from Ti-in-quartz thermometer intersect average quartz-in-garnet isomeke within the P-T range indicated by the intersection of quartz and zircon entrapment isomekes that is $P = 1.8 \pm 0.2$ GPa and $T = 860 \pm 70$ °C.
- The result of the applied two independent approaches of elastic and trace element thermometry showed good agreement with each other. The combined use of Ti-in-quartz thermometry validates zircon-in-garnet elastic thermometry, providing reliable results on entrapment temperature using zircon crystal from Ratanakiri, Cambodia as a natural reference material.
- Quartz and/or zircon crystal inclusions can be commonly entrapped with fluid inclusions coevally. Our study is a good example how elastic thermobarometry provides opportunity to calculate not only the P-T entrapment conditions of crystal inclusion(s), but also those of subduction fluid. Consequently, such indirect application in fluid inclusion studies offers an excellent tool to obtain entrapment conditions of inclusions that cannot be re-homogenized and/or experienced partial H_2O loss during exhumation.

Supplementary data to this article can be found online at https://doi.org/10.1016/j.lithos.2023.107171.

Declaration of Competing Interest

The authors declare that they have no known competing financial interests or personal relationships that could have appeared to influence the work reported in this paper.

Acknowledgements

The authors thank the editor, Prof. Nadia Malaspina and two anonymous reviewers for the careful and constructive comments and suggestions which improved the quality of the manuscript. This work was supported by the NKFIH_FK (no. 132418) research program from the source of the National Research, Development and Innovation Office granted to Márta Berkesi; the MTA FI Lendület FluidsByDepth grant from the source of the Hungarian Academy of Sciences to Márta Berkesi; the ÚNKP-22-4 New National Excellence Program of the Ministry for Innovation and Technology from the source of the National Research, Development and Innovation Fund to Tamás Spránitz. Matteo Alvaro and Mattia Gilio were supported by the European Research Council under the Horizon 2020 Research and Innovation Program for the ERC Starting Grant "TrueDepths" N. 714936 (M.A.) and the PRIN-MUR project "THALES" Prot.2020WPMFE9_003. We also thank for the help of Prof. Sándor Józsa during sampling and Annamária Kis for testing zircon reference crystals. Both the applied zircon reference samples are courtesy of Lutz Nasdala (University of Vienna). This paper is the 117th publication of the Lithosphere Fluid Research Lab.

References

Ábalos, B., Azcarrage, J., Gil Ibarguchi, J.I., Mendia, M.S., Santos Zalduegui, J.S., 1996. Flow stress, strain rate and effective viscosity evaluation in a high-presssure metamorphic nappe (Cabo Ortegal, Spain). J. Metamorph. Geol. 14 (2), 227–248.

Ábalos, B., Puelles, P., Gil Ibarguchi, J.I., 2003. Structural assemblage of high-pressure mantle and crustal rocks in a subduction channel (Cabo Ortegal, NW Spain). Tectonics 22 (2).

Alvaro, M., Mazzucchelli, M.L., Angel, R.J., Murri, M., Campomenosi, N., Scambelluri, M., Nestola, F., Korsakov, A., Tomilenko, A.A., Marone, F., Morana, M., 2020. Fossil subduction recorded by quartz from the coesite stability field. Geology 2019 48 (1), 24–28.

Angel, R.J., Mazzucchelli, M.L., Alvaro, M., Nimis, P., Nestola, F., 2014. Geobarometry from host-inclusion systems: the role of elastic relaxation. Am. Mineral. 99 (10), 2146–2149.

Angel, R.J., Mazzucchelli, M.L., Alvaro, M., Nestola, F., 2017. EosFit-Pinc: a simple GUI for host-inclusion elastic thermobarometry. Am. Mineral. 102 (9), 1957–1960.

Angel, R.J., Murri, M., Mihailova, B., Alvaro, M., 2019. Stress, strain and Raman shifts. Zeitschrift für Kristallograph.-Crystall. Mater. 234 (2), 129–140.

Angel, R.J., Gilio, M., Mazzucchelli, M., Alvaro, M., 2022. Garnet EoS: a critical review and synthesis. Contrib. Mineral. Petrol. 177 (5), 1–22.

Aradi, L.E., Spránitz, T., Guzmics, T., Berkesi, M., 2022. Raman imaging of multiphase fluid inclusions: a case study from the Cabo Ortegal complex, Spain. Goldschmidt Conf. (Hawaii) 10-15 (07), 2022. https://conf.goldschmidt.info/goldschmidt/2022/meetingapp.cgi/Paper/11914.

Bartoli, O., Cesare, B., 2020. Nanorocks: a 10-year-old story. Rendiconti Lincei. Sci. Fisiche e Nat. 31 (2), 249–257.

Beranoaguirre, A., de Madinabeitia, S.G., Lorda, M.S., Puelles, P., Ábalos, B., Gil Ibarguchi, J.I., 2020. U-Pb, Hf isotope and REE constraints on high-pressure acid migmatites from the Cabo Ortegal complex (NW Spain): New evidence of short-duration metamorphism in a Variscan subduction channel. Lithos 372, 105660.

Bodnar, R.J., 2003. Reequilibration of fluid inclusions. In I. Samson, A. Anderson, D. Marshall, eds. Fluid Inclusions: Analysis and Interpretation. Mineral. Assoc. Canada Short Course 32, 213–230.

Bodnar, R.J., Frezzotti, M.L., 2020. Microscale chemistry: Raman analysis of fluid and melt inclusions. Elements: Int. Magaz. Mineral., Geochem., Petrol. 16 (2), 93–98.

Bonazzi, M., Tumiati, S., Thomas, J.B., Angel, R.J., Alvaro, M., 2019. Assessment of the reliability of elastic geobarometry with quartz inclusions. Lithos 350, 105201.

Campomenosi, N., Mazzucchelli, M.L., Mihailova, B., Scambelluri, M., Angel, R.J., Nestola, F., Reali, A., Alvaro, M., 2018. How geometry and anisotropy affect residual strain in host-inclusion systems: Coupling experimental and numerical approaches. American Mineral.: J. Earth and Planet. Mater. 103 (12), 2032–2035.

Campomenosi, N., Rubatto, D., Hermann, J., Mihailova, B., Scambelluri, M., Alvaro, M., 2020. Establishing a protocol for the selection of zircon inclusions in garnet for Raman thermobarometry. American Mineral.: J. Earth and Planet. Mater. 105 (7), 992–1001.

Campomenosi, N., Scambelluri, M., Angel, R.J., Hermann, J., Mazzucchelli, M.L., Mihailova, B., Piccoli, F., Alvaro, M., 2021. Using the elastic properties of zircon-garnet host-inclusion pairs for thermobarometry of the ultrahigh-pressure Dora-Maira whiteschists: problems and perspectives. Contrib. Mineral. Petrol. 176 (5), 1–17.

Campomenosi, N., Angel, R.J., Alvaro, M., Mihailova, B., 2022. Resetting of zircon inclusions in garnet: Implications for elastic thermobarometry. Geology 51 (1), 23–27.

Carvalho, B.B., Bartoli, O., Cesare, B., Tacchetto, T., Gianola, O., Ferri, F., Aradi, L.E., Szabó, C.S., 2020. Primary CO_2-bearing fluid inclusions in granulitic garnet usually do not survive. Earth Planet. Sci. Lett. 536, 116170.

Cesare, B., Acosta-Vigil, A., Bartoli, O., Ferrero, S., 2015. What can we learn from melt inclusions in migmatites and granulites? Lithos 239, 186–216.

Cesare, B., Parisatto, M., Mancini, L., Peruzzo, L., Franceschi, M., Tacchetto, T., Reddy, S., Spiess, R., Nestola, F., Marone, F., 2021. Mineral inclusions are not immutable: evidence of post-entrapment thermally-induced shape change of quartz in garnet. Earth Planet. Sci. Lett. 555, 116708.

Cooke, R.A., 2000. High-pressure/temperature metamorphism in the St. Leonhard Granulite Massif, Austria: evidence from intermediate pyroxene-bearing granulites. Int. J. Earth Sci. 89 (3), 631–651.

Crawford, M.L., Hollister, L.S., 1986. Metamorphic fluids: The evidence from fluid inclusions. In: Fluid—Rock Interactions during Metamorphism. Springer, New York, NY, pp. 1–35.

Ferrando, S., Frezzotti, M.L., Petrelli, M., Compagnoni, R., 2009. Metasomatism of continental crust during subduction: the UHP whiteschists from the Southern Dora-Maira Massif (Italian Western Alps). J. Metamorph. Geol. 27 (9), 739–756.

Ferrero, S., Angel, R.J., 2018. Micropetrology: are inclusions grains of truth? J. Petrol. 59 (9), 1671–1700.
Ferrero, S., Godard, G., Palmeri, R., Wunder, B., Cesare, B., 2018. Partial melting of ultramafic granulites from Dronning Maud Land, Antarctica: Constraints from melt inclusions and thermodynamic modeling. American Mineral.: J. Earth and Planet. Mater. 103 (4), 610–622.
Frezzotti, M.L., Ferrando, S., 2015. The chemical behavior of fluids released during deep subduction based on fluid inclusions. Am. Mineral. 100 (2–3), 352–377.
Frost, B.R., Chacko, T., 1989. The granulite uncertainty principle: limitations on thermobarometry in granulites. J. Geol. 97 (4), 435–450.
Galán, G., Marcos, A., 1997. Geochemical evolution of high-pressure mafic granulites from the Bacariza formation (Cabo Ortegal complex, NW Spain): an example of a heterogeneous lower crust. Geol. Rundsch. 86 (3), 539–555.
Galán, G., Marcos, A., 2000. The metamorphic evolution of the high pressure mafic granulites of the Bacariza Formation (Cabo Ortegal complex, Hercynian belt, NW Spain). Lithos 54 (3–4), 139–171.
Gil Ibarguchi, J.I., Mendia, M., Girardeau, J., Peucat, J.J., 1990. Petrology of eclogites and clinopyroxene-garnet metabasites from the Cabo Ortegal complex (northwestern Spain). Lithos 25 (1–3), 133–162.
Gilio, M., Angel, R.J., Alvaro, M., 2021. Elastic geobarometry: how to work with residual inclusion strains and pressures. American Mineral.: J. Earth and Planet. Mater. 106 (9), 1530–1533.
Gilio, M., Scambelluri, M., Angel, R.J., Alvaro, M., 2022. The contribution of elastic geothermobarometry to the debate on HP versus UHP metamorphism. J. Metamorph. Geol. 40 (2), 229–242.
Gonzalez, J.P., Thomas, J.B., Baldwin, S.L., Alvaro, M., 2019. Quartz-in-garnet and Ti-in-quartz thermobarometry: Methodology and first application to a quartzofeldspathic gneiss from eastern Papua New Guinea. J. Metamorph. Geol. 37 (9), 1193–1208.
Groppo, C., Beltrando, M., Compagnoni, R., 2009. The P–T path of the ultra-high pressure Lago di Cignana and adjoining high-pressure meta-ophiolitic units: insights into the evolution of the subducting Tethyan slab. J. Metamorph. Geol. 27 (3), 207–231.
Hanchar, J.M., Finch, R.J., Hoskin, P.W., Watson, E.B., Cherniak, D.J., Mariano, A.N., 2001. Rare earth elements in synthetic zircon: part 1. Synthesis, and rare earth element and phosphorus doping. Am. Mineral. 86 (5–6), 667–680.
Harlov, D.E., 2012. The potential role of fluids during regional granulite-facies dehydration in the lower crust. Geosci. Front. 3 (6), 813–827.
Hermann, J., Spandler, C., Hack, A., Korsakov, A.V., 2006. Aqueous fluids and hydrous melts in high-pressure and ultra-high pressure rocks: Implications for element transfer in subduction zones. Lithos 92 (3–4), 399–417.
Hermann, J., Zheng, Y.F., Rubatto, D., 2013. Deep fluids in subducted continental crust. Elements 9 (4), 281–287.
Hoskin, P.O., Rodgers, K.A., 1996. Raman spectral shift in the isomorphous series ($Zr_{1-x}Hf_x$) SiO_4. Eur. J. Solid State Inorgan. Chem. 33 (11), 1111–1121.
Jamtveit, B., Austrheim, H., Putnis, A., 2016. Disequilibrium metamorphism of stressed lithosphere. Earth Sci. Rev. 154, 1–13.
Jeanneret, P., Klonowska, I., Barnes, C., Majka, J., Holmberg, J., Gillio, M., Nachlas, W., Alvaro, M., Kosminska, K., Lorenz, H., Zack, T., Ladenberger, A., Koyi, H., 2022. Deciphering the tectonometamorphic history of subducted metapelites using quartz-in-garnet and Ti-in-quartz (QuiG–TiQ) geothermobarometry — a key for understanding burial in the Scandinavian Caledonides. J. Metamorph. Geol. 1–36.
Johnson, T.A., Cottle, J.M., Larson, K.P., 2021. Delineation of multiple metamorphic events in the Himalayan Kathmandu complex, Central Nepal. J. Metamorph. Geol. 39 (4), 443–472.
Kohn, M.J., Mazzucchelli, M.L., Alvaro, M., 2023. Elastic Thermobarometry. Ann. Rev. Earth Planet. Sci. 51 (1) https://doi.org/10.1146/annurev-earth-031621-112720.
Kuzmany, H., 2009. Light scattering spectroscopy. In: Solid-state spectroscopy. Springer, Berlin, Heidelberg, pp. 183–215.
Li, J., Chou, I., 2017. Homogenization experiments of crystal-rich inclusions in spodumene from Jiajika lithium deposit, China, under elevated external pressures in a hydrothermal diamond-anvil cell. Geofluids 2017, 12. Article ID 9252913.
Maffeis, A., Ferrando, S., Connolly, J.A.D., Groppo, C., Frezzotti, M.L., Castelli, D., 2021. Thermodynamic analysis of HP-UHP fluid inclusions: the solute load and chemistryof metamorphic fluids. Geochim. Cosmochim. Acta 315, 207–229.
Malaspina, N., Langenhorst, F., Tumiati, S., Campione, M., Frezzotti, M.L., Poli, S., 2017. The redox budget of crust-derived fluid phases at the slab-mantle interface. Geochim. Cosmochim. Acta 209, 70–84.
Mazzucchelli, M.L., Burnley, P., Angel, R.J., Morganti, S., Domeneghetti, M.C., Nestola, F., Alvaro, M., 2018. Elastic geothermobarometry: Corrections for the geometry of the host-inclusion system. Geology 46 (3), 231–234.
Mazzucchelli, M.L., Angel, R.J., Alvaro, M., 2021. EntraPT: an online platform for elastic geothermobarometry. American Mineral.: J. Earth and Planet. Mater. 106 (5), 830–837.
Murri, M., Mazzucchelli, M.L., Campomenosi, N., Korsakov, A.V., Prencipe, M., Mihailova, B.D., Scambelluri, M., Angel, R., Alvaro, M., 2018. Raman elastic geobarometry for anisotropic mineral inclusions. American Mineral.: J. Earth and Planet. Mater. 103 (11), 1869–1872.
Nasdala, L., Lengauer, C.L., Hanchar, J.M., Kronz, A., Wirth, R., Blanc, P., Seydoux-Guillaume, A.M., 2002. Annealing radiation damage and the recovery of cathodoluminescence. Chem. Geol. 191 (1–3), 121–140.
Nasdala, L., Akhmadaliev, S., Artac, A., Chanmuang, N.C., Habler, G., Lenz, C., 2018. Irradiation effects in monazite–(Ce) and zircon: Raman and photoluminescence study of Au-irradiated FIB foils. Phys. Chem. Miner. 45 (9), 855–871.
Newton, R.C., Aranovich, L.Y., Hansen, E.C., Vandenheuvel, B.A., 1998. Hypersaline fluids in Precambrian deep-crustal metamorphism. Precambrian Res. 91 (1–2), 41–63.
O'Brien, P.J., 2001. Subduction followed by collision: Alpine and Himalayan examples. Phys. Earth Planet. Inter. 127 (1–4), 277–291.
O'Brien, P.J., 2008. Challenges in high-pressure granulite metamorphism in the era of pseudosections: reaction textures, compositional zoning and tectonic interpretation with examples from the Bohemian Massif. J. Metamorph. Geol. 26 (2), 235–251.
O'Brien, P.J., Rötzler, J., 2003. High-pressure granulites: formation, recovery of peak conditions and implications for tectonics. J. Metamorph. Geol. 21 (1), 3–20.
Ordóñez Casado, B.O., Gebauer, D., Schäfer, H.J., Gil Ibarguchi, J.I., Peucat, J.J., 2001. A single Devonian subduction event for the HP/HT metamorphism of the Cabo Ortegal complex within the Iberian Massif. Tectonophysics 332 (3), 359–385.
Özkan, H., Cartz, L., Jamieson, J.C., 1974. Elastic constants of nonmetamict zirconium silicate. J. Appl. Phys. 45 (2), 556–562.
Puelles, P., Ábalos, B., Gil Ibarguchi, J.I., 2005. Metamorphic evolution and thermobaric structure of the subduction-related Bacariza high-pressure granulite formation (Cabo Ortegal complex, NW Spain). Lithos 84 (1–2), 125–149.
Rajesh, H.M., Santosh, M., 2012. Charnockites and charnockites. Geosci. Front. 3, 737–744.
Santos, J.F., Schärer, U., Gil Ibarguchi, J.I., Girardeau, J., 2002. Genesis of pyroxenite-rich peridotite at Cabo Ortegal (NW Spain): geochemical and Pb–Sr–Nd isotope data. J. Petrol. 43 (1), 17–43.
Scambelluri, M., Philippot, P., 2001. Deep fluids in subduction zones. Lithos 55 (1–4), 213–227.
Spear, F.S., Florence, F.P., 1992. Thermobarometry in granulites: pitfalls and new approaches. Precambrian Res. 55 (1–4), 209–241.
Spear, F.S., Ashley, K.T., Webb, L.E., Thomas, J.B., 2012. Ti diffusion in quartz inclusions: implications for metamorphic time scales. Contrib. Mineral. Petrol. 164 (6), 977–986.
Spear, F.S., Wolfe, O.M., Cheney, J.T., 2023. On the interpretation of TitaniQ and ZiR thermobarometry in subduction complexes. Contrib. Mineral. Petrol. 178, 8 (2023).
Spránitz, T., Padrón-Navarta, J.A., Szabó, Cs, Szabó, Á., Berkesi, M., 2022. Abiotic passive nitrogen and methane enrichment during exhumation of subducted rocks: primary multiphase fluid inclusions in high-pressure rocks from the Cabo Ortegal complex, NW Spain. J. Metamorph. Geol. 40 (8), 1291–1319.
Stangarone, C., Angel, R.J., Prencipe, M., Campomenosi, N., Mihailova, B., Alvaro, M., 2019. Measurement of strains in zircon inclusions by Raman spectroscopy. Eur. J. Mineral. 31 (4), 685–694.
Sterner, S.M., Bodnar, R.J., 1989. Synthetic fluid inclusions-VII. Re-equilibration of fluid inclusions in quartz during laboratory-simulated metamorphic burial and uplift. J. Metamorph. Geol. 7 (2), 243–260.
Taylor, J., 1997. Introduction to Error Analysis, 2nd edition. University Science Books, Sausalito, CA, USA, p. 1997.
Thomas, J.B., Bruce Watson, E., Spear, F.S., Shemella, P.T., Nayak, S.K., Lanzirotti, A., 2010. TitaniQ under pressure: the effect of pressure and temperature on the solubility of Ti in quartz. Contrib. Mineral. Petrol. 160 (5), 743–759.
Tilhac, R., Grégoire, M., O'Reilly, S.Y., Griffin, W.L., Henry, H., Ceuleneer, G., 2017. Sources and timing of pyroxenite formation in the sub-arc mantle: Case study of the Cabo Ortegal complex, Spain. Earth Planet. Sci. Lett. 474, 490–502.
Touret, J.L.R., 2009. Mantle to lower-crust fluid/melt transfer through granulite metamorphism. Russ. Geol. Geophys. 50 (12), 1052–1062.
Tual, L., Möller, C., Whitehouse, M.J., 2018. Tracking the prograde P–T path of Precambrian eclogite using Ti-in-quartz and Zr-in-rutile geothermobarometry. Contrib. Mineral. Petrol. 173 (7), 1–15.
Vogel, D.E., 1967. Petrology of an eclogite-and pyrigarnite-bearing polymetamorphic rock complex at Cabo Ortegal, NW Spain. Leidse. Geol. Meded. 40 (1), 121–213.
Wang, J., Mao, Z., Jiang, F., Duffy, T.S., 2015. Elasticity of single-crystal quartz to 10 GPa. Phys. Chem. Miner. 42, 203–212.
Zeug, M., Nasdala, L., Wanthanachaisaeng, B., Balmer, W.A., Corfu, F., Wildner, M., 2018. Blue Zircon from Ratanakiri, Cambodia. J. Gemmol. 36, 112–132.
Zhang, Z.M., Shen, K., Sun, W.D., Liu, Y.S., Liou, J.G., Shi, C., Wang, J.L., 2008. Fluids in deeply subducted continental crust: petrology, mineral chemistry and fluid inclusion of UHP metamorphic veins from the Sulu orogen, eastern China. Geochim. Cosmochim. Acta 72 (13), 3200–3228.
Zhong, X., Moulas, E., Tajčmanová, L., 2018. Tiny timekeepers witnessing high-rate exhumation processes. Sci. Rep. 8 (1), 1–9.
Zhong, X., Andersen, N.H., Dabrowski, M., Jamtveit, B., 2019. Zircon and quartz inclusions in garnet used for complementary Raman thermobarometry: application to the Holsnøy eclogite, Bergen Arcs, Western Norway. Contrib. Mineral. Petrol. 174 (6), 1–17.
Zhong, X., Moulas, E., Tajčmanová, L., 2020. Post-entrapment modification of residual inclusion pressure and its implications for Raman elastic thermobarometry. Solid Earth 11 (1), 223–240.